Direct Numerical Simulation of Interaction between Transient Flow and Blade Structure in a Modern Low-Pressure Turbine

Shine Win Naung*, Mohammad Rahmati, Hamed Farokhi

Department of Mechanical and Construction Engineering, Northumbria University, Newcastle upon Tyne, United Kingdom, NE1 8ST

* Corresponding author
Email: shine.naung@northumbria.ac.uk

ABSTRACT

A feature of a modern aeronautical Low-Pressure Turbine (LPT) is the high blade loadings with complex, transient and separated flow regimes. Most existing research have focused only on analysing the transient flow and flow separation in such turbines. The aerodynamics of a modern LPT, however, can be significantly influenced by the interaction between the unsteady flow field and the blade structure motion in a complex non-linear fashion which could lead to aeroelastic instabilities such as flutter. Therefore, the understanding of the mechanism of the interaction between the flow field unsteadiness and the blade structure in a modern LPT is essential to examine the vibration stress levels to ensure the blade mechanical integrity. The novelty of this paper, first and foremost, is using a high-fidelity direct numerical simulation method to explore the mechanism of flutter and forced response in a modern LPT, T106A turbine, and to study the effects of various sources of unsteadiness on the aeroelastic instabilities of the blade. Secondly, this paper investigates and identifies the adequate working ranges of the harmonic balance method, which has been widely used for the aeromechanical analysis of turbomachines, on predicting the behaviour of the highly unsteady flow due to fluid-structure interaction in an LPT. Another emphasis of this paper is the determination of the capability of the Unsteady Reynolds Averaged Navier–Stokes (URANS) model for the aeroelasticity analysis of an LPT involving the highly unsteady flow. This paper will bridge a key gap in the knowledge of aeroelasticity modelling and analysis of modern LPTs.

Keywords

low-pressure turbines, aerodynamics, aeroelasticity, computational fluid dynamics, direct numerical simulation method, harmonic balance method, fluid-structure interaction

NOMENCLATURE

U	-	Vectors of the conservative variables
τ	-	Stress tensor
S_M	-	Momentum source term
R	-	Lumped residual and source term
$\overline{U}$	-	Fourier coefficient of the conservative variables
A_m	-	Fourier coefficient of the conservative variables
B_m	-	Fourier coefficient of the conservative variables
ω	-	Vibration frequency
m	-	Number of harmonics
Δt	-	time-step size
C_{FL}	-	CFL number
u_{inlet}	-	Inlet velocity
u_x	-	Velocity in the stream-wise direction
u_y	-	Velocity in the pitch-wise direction
u_z	-	Velocity in the span-wise direction
q	-	Generalized displacement
$\bar{q}$	-	Mean value of generalized displacement
q_A	-	Amplitude of generalized displacement
d	-	Global displacement of the blade structure
$\bar{d}$	-	Mean value of the blade displacement

d_A -   Amplitude of the blade displacement

ϕ -   Structural mode shape

C_p -   Pressure coefficient

p_w -   Wall static pressure

p_{ref} -   Reference pressure

$p_{t\text{-}in}$ -   Inlet total pressure

p_t -   Total pressure

ω_u -   Wake deficit

C_{ax} -   Axial chord length

1. INTRODUCTION

Unsteady flows through various blade rows often influence the aerodynamic performance of turbomachines [1]. The interaction between the unsteady flow and the dynamic behaviour of a structure can influence the flow unsteadiness behind the structure [2], potentially leading to either an instantaneous or a high cycle fatigue (HCF) failure of a structure. Most of the modern civil aero engines consist of the Low-Pressure Turbine (LPT) which can account for approximately 20-30 percent of the total engine weight [3]. The flow inside an LPT in aero engines is prone to separation due to the low air density resulting in a low Reynolds number. Several studies have been performed to improve the efficiency of the LPTs and, as a result, the high levels of efficiency (90-93%) has been achieved [4,5].

After having achieved the optimum and satisfactory level of efficiency, the focus of the studies has now shifted towards reducing the weight and the associated manufacturing costs of the LPTs [6]. A significant effort was devoted to producing a 'high-lift' blade design which increases the aerodynamic loads on the blade. This design ensures that the required stage

loading is achieved using a smaller number of blades, thereby reducing the total weight [7]. However, these designs not only decrease the highly correlated LPT flutter parameter known as reduced frequency but also introduce the higher per-stage loading [8-10], which could introduce aeroelastic instabilities such as flutter. Although the flutter and forced response has been a problem traditionally associated with the compressors and fans of gas turbines, the LPTs of modern gas turbines may also be prone to the aeroelastic instability problems similar to those encountered in the compressors and fans due to the high loading conditions in a combination with an increase of the blade aspect ratio and reducing the blade thickness [11]. The aeroelastic instability problems are also linked with the fatigue and fracture of the blade structure [12]. This triggers further studies to be carried out to develop numerical methods and tools to investigate the physics of onset of flutter for the LPTs in order to examine the vibration stress levels and to ensure the blade mechanical integrity.

As an accurate prediction of flutter and forced response in turbomachines, especially in LPTs, is one of the greatest unsolved challenges faced by the industry, a lot of efforts have been made over the last decades to seek efficient numerical methods. One of them is the time-linearized harmonic frequency-domain method which has been developed and widely used for turbomachinery aeromechanical applications [13-14]. However, these methods were superseded by the harmonic balance method of Hall et al. [15], the phase solution method of He [16], and Rahmati et al. [17-18] which provide a particularly elegant way of modelling harmonic disturbances. Rahmati et al. [19] developed a harmonic balance method for the turbomachinery aeromechanical analysis and design of multiple blade row configurations. It is shown that a fully coupled multi-row analysis should yield more accurate flutter predictions than the simplified isolated blade row case [20]. Shine et al. [21-22] also applied the non-linear harmonic method to the aerodynamic and aeromechanical analysis of wind turbine rotors.

Breard et al. [23] proposed an integrated aeroelasticity model to predict the forced responses of a high-pressure turbine blade based on a two-way coupling approach. However, the existing high-fidelity aeroelasticity models are based on the Unsteady Reynolds Averaged Navier–Stokes (URANS) equations. URANS models are often used in the industry to study unsteady flows [24-25]. As discussed by Tucker [26-28], the URANS models are not capable of predicting the unsteady flow behaviour, especially in the flow separation zone due to the interaction between the transient flow and the blade structure, which is usually seen in LPTs. Therefore, the required confidence and accuracy cannot be obtained with the URANS models because of the inadequacy of the turbulence models. The existing aeroelasticity models and solvers used in the industry mainly focus on the aeroelasticity parameters such as the value of aerodynamic damping or the structural responses but disregards the complex physics occurring during the fluid-structure interaction process which gives rise to a black-box effect. As a result, the understanding of the interaction between the various sources of unsteadiness and the blade structure is still limited, and it requires further investigations. Therefore, a high-fidelity numerical model should be developed to provide an understanding of the physics behind fluid-structure interactions.

Direct Numerical Simulations (DNSs) are highly efficient and they can provide a detailed insight into the physics of turbulence. However, the computational resources required by a DNS simulation are extremely high and sometimes can exceed the capability of powerful computers. Due to recent technical and computational advances, DNS has become more feasible and it has been applied in different engineering applications [29-33]. The overarching aim of this paper is to explore the forced response and flutter instability in a modern LPT using a high-fidelity DNS method in which the various sources of unsteadiness associated with the fluid-structure interaction are included. To the best of the authors' knowledge, all research to

date have focused only on the transient flow and flow separation in modern aeronautical LPTs. The present work will provide fundamental understandings of the mechanism behind the interaction between the flow field unsteadiness and the blade structure in a modern LPT. This work will bridge a key gap in the knowledge of aeroelasticity modelling and prediction, and results will be relevant to other turbomachines prone to aeroelastic instabilities such as steam turbines and wind turbine blades.

2. T106A LINEAR TURBINE CASCADE

The highly loaded T106A linear turbine cascade has been selected for the present study. This turbine has been studied both experimentally [34] and numerically [35-43]. The experimentally studied test rig consists of seven aft-loaded blades. A single passage domain with a blade at the middle and periodic boundary conditions are used for the present numerical investigations. The blade aspect ratio and pitch-to-chord ratio are 1.76 and 0.799, respectively. The experimental measurements of this turbine were performed at a relatively low Reynolds number of 51,800 with an inflow angle of 37.7 degrees. The required Reynolds number is obtained based on the inflow speed and the axial chord length in the present simulations. However, it should be noted that the inflow angle for the numerical simulations is shifted to 45.5 degrees due to some uncertainties in the experiment as explained by Michelassi et al. [42-43]. The time-averaged pressure coefficient distribution and the wake loss profile in a cross-section downstream of the blade trailing edge were measured during the experiment, and they will be compared to the numerical results for validation purposes. Besides, the wall shear stress on the blade surfaces is also computed and compared to the reference DNS simulation. Titanium Alloy is considered to be the material of the blade in this study and it has a density of $4620 \, \text{kg/m}^3$, Young's modulus of 9.6E+10 Pa and Poisson's ratio of 0.36.

## 3. DIRECT NUMERICAL SIMULATION

3.1 Computational Domain and Grid

The computational domain, shown in Fig. 1 (a), is created to simulate the flow at the mid-span section of the T106A LPT cascade where the flow is two-dimensional. It is important to ensure that the entire domain is optimal in all stream-wise, pitch-wise and span-wise directions to capture and resolve the necessary flow structures. The span-wise extension used in this paper is $0.2C_{ax}$ where C_{ax} is the axial chord length. Previous studies [37-43] suggest that $0.2C_{ax}$ or $0.15C_{ax}$ should be sufficient to capture the separated flow transition. Therefore, the span-wise length of $0.2C_{ax}$ is considered enough in this study. Moreover, the wake profiles are investigated at the section of 40% chord downstream of the trailing edge in the experiment as well as the numerical studies, and therefore the outlet of the domain is placed $2C_{ax}$ from the trailing edge of the blade in this study to fully resolve the downstream wake region. Although the length of $1C_{ax}$ is enough, which is mostly used in previous studies, that of $2C_{ax}$ ensures that the downstream wakes and flow structures are captured which is particularly important when the blade vibration is involved. The same length from the leading edge of the blade is used for the inlet. In the pitch-wise direction, the pitch length is $0.9306C_{ax}$, which is consistent with the experiment and other studies. Therefore, the domain used in this study is considered adequate in all directions for the present study.

The grid employed in this study is carefully generated using a structured grid generator, NUMECA AutoGrid5, based on structured multi-block techniques to be suitable for DNS computations. The O4H topology is used to create the grid which consists of five blocks – the skin block which is an O-mesh surrounding the blade, the inlet block which is an H-mesh located upstream of the leading edge, the outlet block which is an H-mesh located downstream of the trailing edge, the upper block which is an H-mesh located above the blade section, and

the lower block which is an H-mesh located under the blade section. The mesh in the skin block, the upper block, the lower block and the outlet block are significantly refined to resolve the necessary flow structures. As a steady inflow is only considered in this study, a coarser mesh is generated in the inlet block to reduce the total number of cells and the computation time. The first layer thickness, which is the width of the first cell close to the wall, is selected with care to capture the flow phenomena inside the boundary layers. The non-dimensional wall distance, y^+ value, is less than one in this study and the final grid has 13.5 million grid points. It should be noted that, before generating this grid, the authors tested different grid sizes with the total grid points of 4.5 million (coarse mesh) and 18 million (fine mesh) and investigated the differences in predicting pressure distributions over the blade surfaces and wake profiles. The latter is similar in grid size as well as gird point distributions to those of Wissink et al. [38] and Michelassi et al. [42-43]. It is found that only a slight difference is seen between the coarse mesh and the fine mesh in terms of the pressure distribution over the blade surfaces. However, a great difference is observed in capturing the wakes as the difference in wake profiles between the two grids is accounted for 20%. The wakes and the flow structures are sufficiently captured and resolved with the fine mesh. As this study does not include inflow wakes, it should be possible that the coarse mesh can be used in the inlet block which could reduce the total number of grid points as well as the computation time. This leads to the final grid size of 13.5 million without compromising the accuracy in capturing the wakes in the downstream region. The final grid is still greater in size than that of Garai et al. [36]. Figure 1 (b) shows the representative coarse mesh at the blade mid-span section.
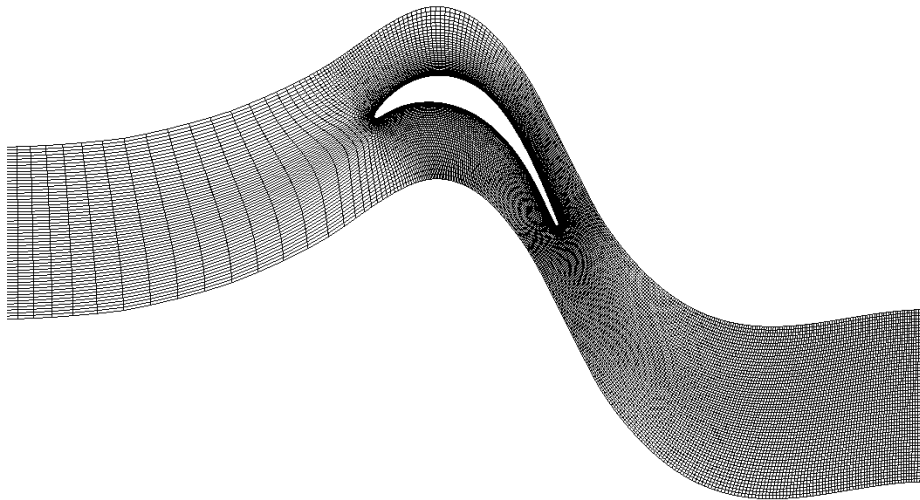
(a)
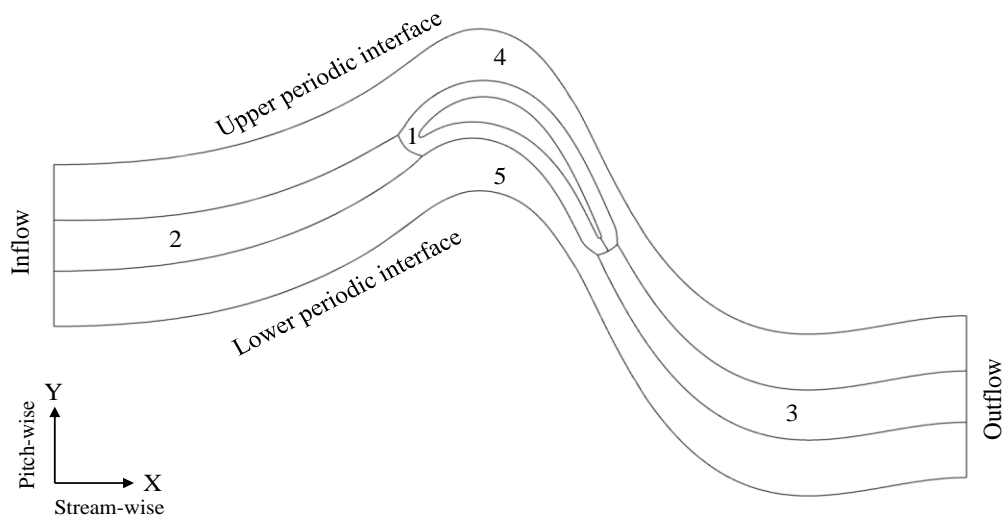
(b)

Figure 1. (a) Computational domain: *1 – skin block, 2 – inlet block, 3 – outlet block, 4 – upper block, 5 – lower block*, and (b) representative computational grid at the blade mid-span section of the T106A turbine

3.2 Computational Methods

The analysis of unsteady flow using the stationary blade is initially performed with the purpose of validating the CFD model. After validation, the blade is imposed a vibration with a

frequency and amplitude to initiate the flutter instability in T106A turbine and to analyse the interaction between the transient flow and the blade structure vibration. The first vibration mode is approximated by imposing a periodic displacement in the pitch-wise direction on the blade. Both the time domain method and the harmonic balance method are used for the unsteady simulations using the vibrating blade. By using the same numeric for both methods, the capability of the harmonic balance method on analysing the forced response and flutter instability in modern LTPs involving highly unsteady flow can be determined. The primary flow simulations are conducted using the DNS method. However, the results from the URANS model will also be added to the comparison in the case using the vibrating blade to investigate the differences between the DNS model and the URAN model, and to identify their capabilities.

The flow is governed by the Navier-Stokes equations and a set of the unsteady Navier-Stokes equations are solved by a three-dimensional pressure-based finite volume solver, ANSYS CFX. The equations of mass and momentum conservation can be written as follow:

$$\frac{\partial \rho}{\partial t} + \nabla . (\rho U) = 0 \tag{1}$$

$$\frac{\partial (\rho U)}{\partial t} + \nabla . (\rho U \otimes U) = -\nabla p + \nabla . \tau + S_M \tag{2}$$

where U is the vector of the conservative variables, τ is the stress tensor and S_M is the momentum source term, respectively. The above equations can be simply written in a semi-discrete form as:

$$\frac{\partial}{\partial t}(U) = R(U) \tag{3}$$

where R is the lumped residual and the source term. With the DNS method, the Navier-Stokes equations are directly solved without any turbulence model. The pseudo-time marching approach is used for the steady-state solution. For the unsteady solution, the advection terms are discretized using a bounded high-resolution advection scheme and the temporal derivatives are discretized using a 2nd order backwards Euler approximation for the time domain method.

In the cases of the flutter and forced response instability problems of the turbomachinery, the source of unsteadiness of the flow is mainly due to blade vibration. Therefore, in this study, the unsteadiness of the flow is associated with the frequency and amplitude of the blade oscillation. As the blade is periodically vibrating, the unsteady flow variables, U, can be represented by a Fourier series, based on the harmonic method, for a prescribed fundamental frequency, ω, and the specified number of harmonics, m, as expressed in Eq. (4).

$$U = \bar{U} + \sum_{m=1}^{M}[A_m \sin(m\omega t) + B_m \cos(m\omega t)] \tag{4}$$

where $\bar{U}$, A_m, and B_m are the Fourier coefficients of the conservation variables. Substituting Eq. (4) into Eq. (3) yields the following equations.

$$\omega \sum_{m=1}^{M}[mA_m \cos(m\omega t) - mB_m \sin(m\omega t)] = R \tag{5}$$

The harmonic balance method, typically used in the turbomachinery analysis, is also implemented in this paper with a pressure-based solution approach to identify its capability. Using this method, the unsteady period is equally divided into $N = (2m+1)$ time levels and the system of nonlinear equations coupling all N time levels are solved iteratively. In this method, the time derivatives are evaluated using the spectral approximation.

To resolve the unsteady flow accurately, the time-step size, Δt, must be small enough such that a fluid particle moves only a fraction of the mesh spacing h with fluid velocity u in each step, and it is given by [44]:

$$\Delta t = C_{FL} \frac{h}{u} \tag{6}$$

where C_{FL} is the CFL number and it is kept in the range of 0.5-1 throughout the computation to ensure a very small time-step which leads to Δt of 10^{-5}.

3.3 Boundary Conditions

For the simulations discussed in this paper, the velocity inflows are applied at the inlet and the pressure outlet boundary condition is defined at the outlet. The solid wall boundary conditions are applied on the blade surfaces. The periodic boundary conditions are applied in the pitch-wise direction and the mirror boundary conditions are applied in the span-wise direction. The details of the boundary conditions are described below.

3.3.1 Inlet

A velocity inlet boundary condition is defined where the flow enters the domain. As there is an inflow angle, the velocity components are specified in the Cartesian frame of reference as follow:

$$u_{inlet} = \sqrt{u_x{}^2 + u_y{}^2} \tag{7.a}$$

$$u_x = u_{inlet}\cos(45.5) \tag{7.b}$$

$$u_y = u_{inlet}\sin(45.5) \tag{7.c}$$

u_{inlet} is calculated based on the required Reynolds number of 51,800 and the axial chord length, and the Z-component of the velocity (i.e. velocity in the span-wise direction), u_z, is zero.

3.3.2 Outlet

A pressure outlet boundary condition is defined where the flow leaves the domain. The atmospheric pressure of 1 atm is specified at the outlet.

3.3.3 Wall

A no-slip wall boundary condition is defined over the blade surfaces. Stationary wall boundary is specified in the stationary blade case whereas the deforming wall boundary with a periodic displacement is specified in the vibrating blade case. In the case of the vibrating blade, the global displacement of the blade structure is defined as:

$$d = q\phi \tag{8}$$

where q is the generalized displacement and ϕ is the structural mode shape of the blade which needs to be imported before the flow simulation. The generalized displacement q can be specified for the considered amplitude of vibration and it can be written as:

$$q(t) = \bar{q} + q_A \sin(\omega t) \tag{9}$$

where $\bar{q}$ and q_A are the mean value and the amplitude of the generalized displacement, respectively, which define the blade vibration.

3.3.4 Mirror and Periodicity

The symmetry boundary condition is specified on each side of the domain in the span-wise direction so that the flow on one side of the domain is the mirror image of that of the other side. The translational periodicity is implemented in the pitch-wise direction to represent a straight row of turbine blades of the linear cascade.

4. RESULTS

4.1 Analysis of Unsteady Flow using the Stationary Blade

Before analysing the effect of the blade structure vibration on the unsteady flow, the unsteady simulation using the stationary blade is first conducted to validate the CFD model. The numerical results are compared to the experiment as well as the reference DNS simulations for validation. The time-averaged static pressure coefficient, C_p, can be defined as $(p_w - p_{ref})/(p_{t\text{-}in}\text{-}p_{ref})$, where p_w is the blade wall static pressure, p_{ref} is the reference outlet pressure, and $p_{t\text{-}in}$ is the inlet total pressure. The time-averaged C_p distribution computed from the present simulation is compared to the experiment as well as the previous DNS simulation performed by Wissink et al. [38], and they are presented in Fig. 2. As seen, the pressure computed from the present simulation is in very good agreement with the experiment as well as the reference DNS simulation.
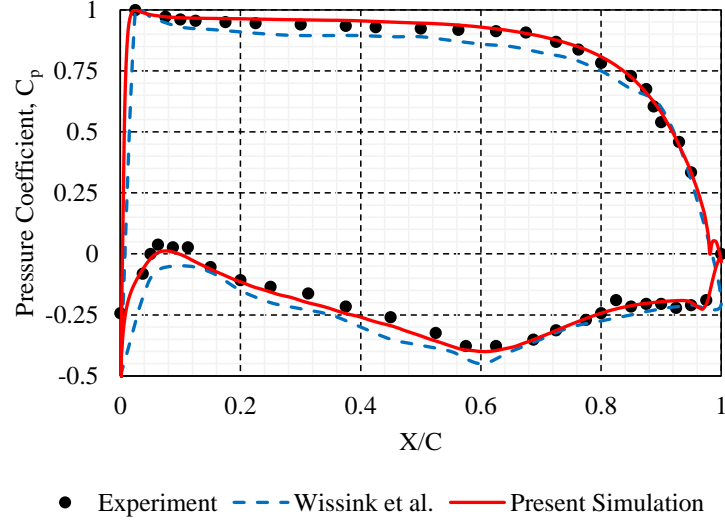
14

Figure 2. Time-averaged pressure coefficient distribution at the blade mid-span obtained from the experiment *(symbol)*, reference DNS simulation of Wissink et al. [38] *(dotted line)* and the present DNS simulation *(line)*

The wake loss profile, also called as wake deficit, ω_u, can be defined as $(p_{t\text{-}in}\text{-}p_t)/(p_{t\text{-}in}\text{-}p_{ref})$, where p_t is the total pressure, and it is computed at 40% chord downstream of the blade trailing edge. Similar to C_p, the time-averaged wake loss profile calculated from the present simulation is compared to the experiment as well as the DNS simulation conducted by Michelassi et al. [42], and they are shown in Fig. 3. A slight difference can be seen between the DNS computations and the experiment. This has been discussed in previous studies [36,42]. Overall, a good agreement is obtained between the present simulation and the experiment, and the results are close to that of Michelassi et al. [42]. Therefore, it can be noted that the present CFD model captured the wake loss reasonably well and this is considered enough for further investigations involving the blade vibration.
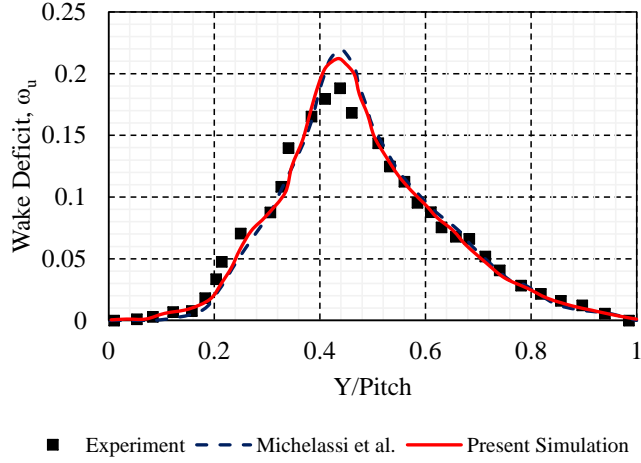
Figure 3. Wake loss profiles at 40% chord downstream of the blade trailing edge obtained from the experiment *(symbol)*, reference DNS simulation of Michelassi et al. [42] *(dotted line)* and the present DNS simulation *(line)*

In addition to the pressure coefficient distribution and the wake loss profile, the shear stresses on the blade surfaces are also computed, and they are compared to the previous DNS simulation performed by Michelassi et al. [42], and they can be seen in Fig. 4. As shown, they are in very good agreement. Therefore, it is concluded that the CFD model used in the present study is valid for further investigations after having obtained the results which agree well with the experiment as well as the reference DNS simulations.
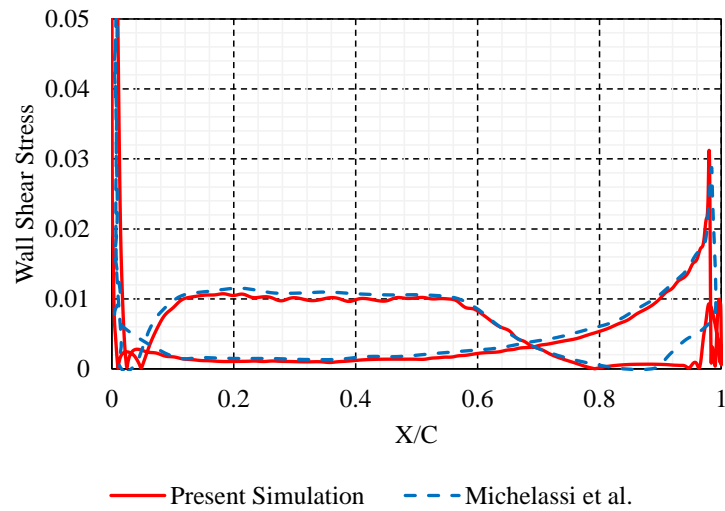
Figure 4. Wall shear stress on the blade surfaces at the blade mid-span obtained from the present DNS simulation *(line)* and the reference DNS simulation of Michelassi et al. [42] *(dotted line)*
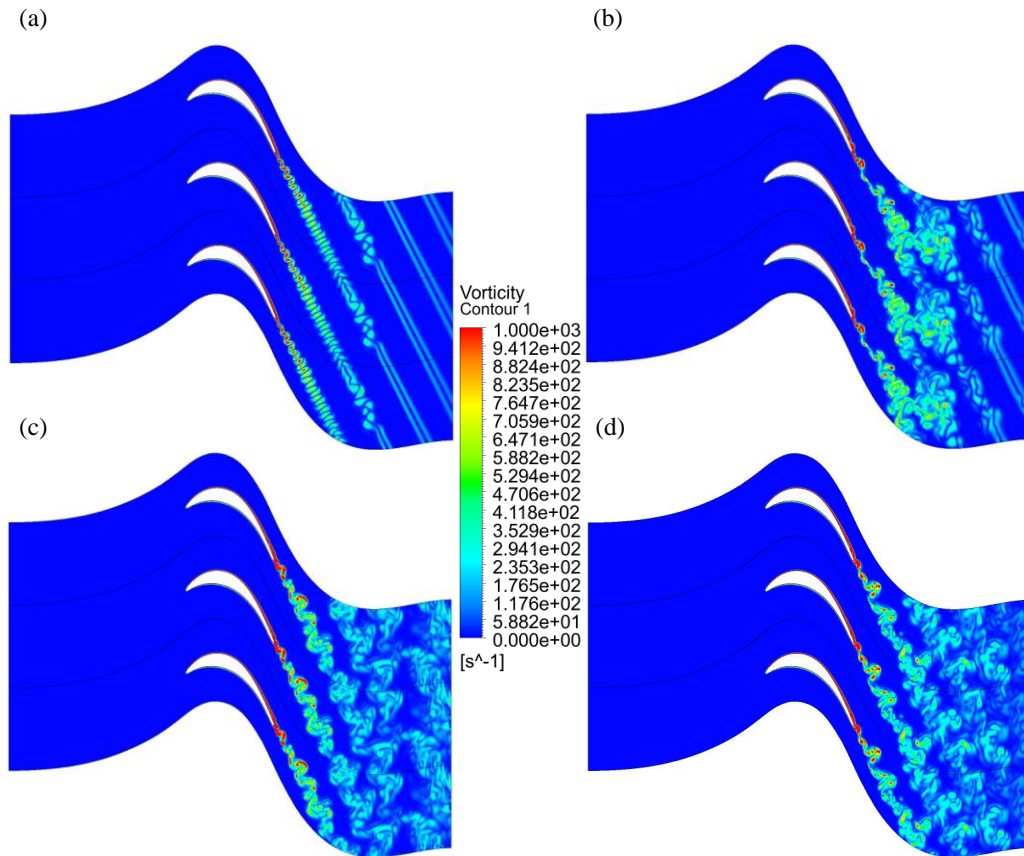
Figure 5. Instantaneous vorticity fields obtained at: (a) t/T = 0.25, (b) t/T = 0.50, (c) t/T = 0.75, and (d) t/T = 1 *(t is the local time-step and T is the total simulation time)*

After having validated the CFD model in terms of the time-averaged parameters, it is also crucial to visualise and analyse the vorticity to determine whether this model captures the necessary flow structures, which is very important for this study. Figure 5 illustrates the instantaneous vorticity structures, at four equally spaced time-steps, obtained from the present simulation. Although a single passage domain is simulated in this study, the additional two passages are added and shown for better visualisation of the flow structures. As seen, on the pressure side of the blade, the flow remains laminar and attached whereas the flow separates in the aft region on the suction side which leads to laminar vortex-shedding from the trailing edge of the blade of which the flow structures are similar to that of Karman vortex. As time goes on, the evolution of coherent structures and separation of shear layers can be observed.

17

The rolling up and breaking down of the separated shear layer occur due to Kelvin-Helmholtz instability which results in a transition to turbulence near the trailing edge and forming unsteady and complex vortex structures further downstream. After a certain period, the flow structure is stretched near the trailing edge and the organised mushroom-like vortex structures are developed to form a fully turbulent wake in the downstream region.

4.2 Analysis of Interaction between Transient Flow and Blade Structure Vibration

To explore the forced response and flutter instability in a modern LPT due to the interaction of unsteady flow and the blade structure, the blade is prescribed a vibration with a frequency and amplitude in the flow simulation. The first vibration mode is approximated by imposing a periodic displacement in the pitch-wise direction on the blade as shown in Fig. 6 and is used in this analysis. This means that each node of the blade has the same displacement and the blade periodically moves up and down, in the Y-direction, with a prescribed frequency and amplitude throughout the run. The global displacement of the blade can be written, based on Eq. (8) and Eq. (9), as:

$$d(t) = \bar{d} + d_A \sin(\omega t) \tag{10}$$

where $\bar{d}$ and d_A are the mean value and amplitude of the blade displacement. The first natural frequency, 250 Hz, obtained from the modal analysis, is adopted to be the vibration frequency in this case. In the aeromechanical analysis of turbomachines, the vibration amplitudes of 1-3%C_{ax} are typically used in both experimental and numerical studies [19-20,45-46]. As this paper only simulates the flow at the mid-span section of the blade, a relatively small amplitude of 1%C_{ax} is considered and set to be the vibration amplitude.
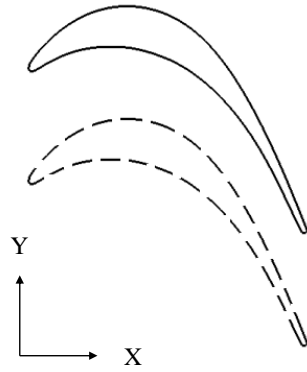
Figure 6. Schematic diagram of the blade vibration showing the blade moving in the pitch-wise direction

The time-averaged pressure coefficient distribution computed from this analysis is first compared to the stationary blade case, and they are shown in Fig. 7. In terms of pressure coefficient distributions on the blade surfaces, only a slight difference is seen between the two cases. This is understandable as the blade displacement is periodic in time and the time-averaged pressure distribution due to the vibration can be similar to that of the stationary case. However, it should be noted that this effect is also related to the frequency and amplitude of the vibration. A little pressure fluctuation due to the flow separation on the suction surface is also observed near the trailing edge.
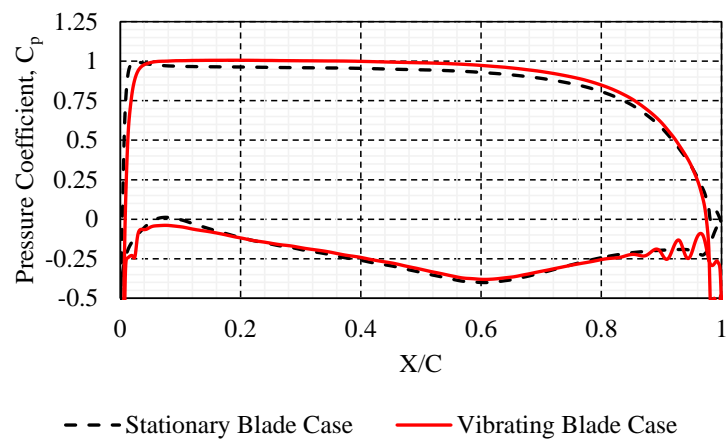

Figure 7. The comparison of time-averaged pressure coefficient distributions between the stationary blade case *(dotted line)* and the vibrating blade case *(line)*

The effect of vibration on the unsteady flow can be clearly observed in the wake profiles (See Figure 8). They are computed at the same location as discussed in the stationary case. A significant difference can be seen between the two cases as the flow is disturbed by the blade vibration. The blade experiences acceleration and deceleration on both pressure and suction surfaces due to the vibration, which leads to an increase and decrease in total pressure in the downstream region. This results in negative and positive wake profiles, as seen in Fig. 8, and the magnitude of the wake is also much larger in the vibrating blade case compared to the stationary blade case.
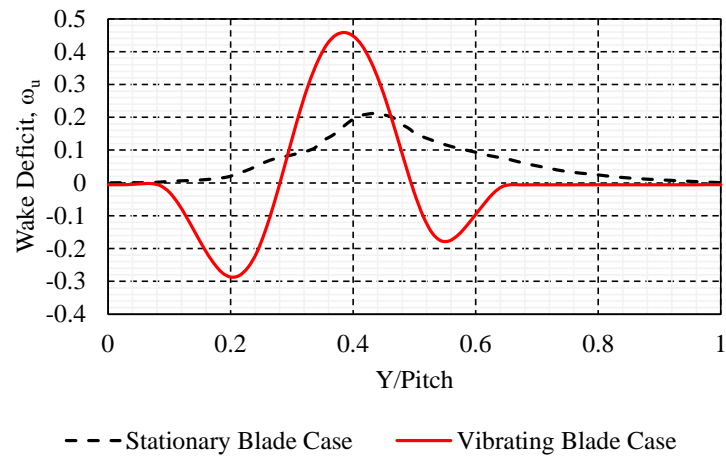
Figure 8. The comparison of wake profiles between the stationary blade case *(dotted line)* and the vibrating blade case *(line)*

The evolution process of vorticity over vibration periods is demonstrated in Fig. 9 which allows visualising the mechanism of the interaction between the flow unsteadiness and the blade structure vibration. As soon as the blade undergoes vibration, the blade structure motion triggers disturbances and the vortex structures shed from the blade trailing edge. The blade produces similar vortex structures as vibration goes on and the initially produced vortex structures are pushed away by the latterly produced ones. After about 20 vibration periods, some of the vortex structures are mixed up with those from the neighbouring blades. The

breaking down and mixing up of vortex structures are clearly observed beyond 30 vibration periods. As vibration periods go on, the highly unsteady vortex structures and completely turbulent flow fields are seen in the downstream region. Overall, it is seen that the flow is predominantly distorted by the blade movement and the periodically moving blade causes the recurring pattern of vortex formation from the trailing edge of the blade. The frequency of vorticity is determined by the blade vibration frequency.
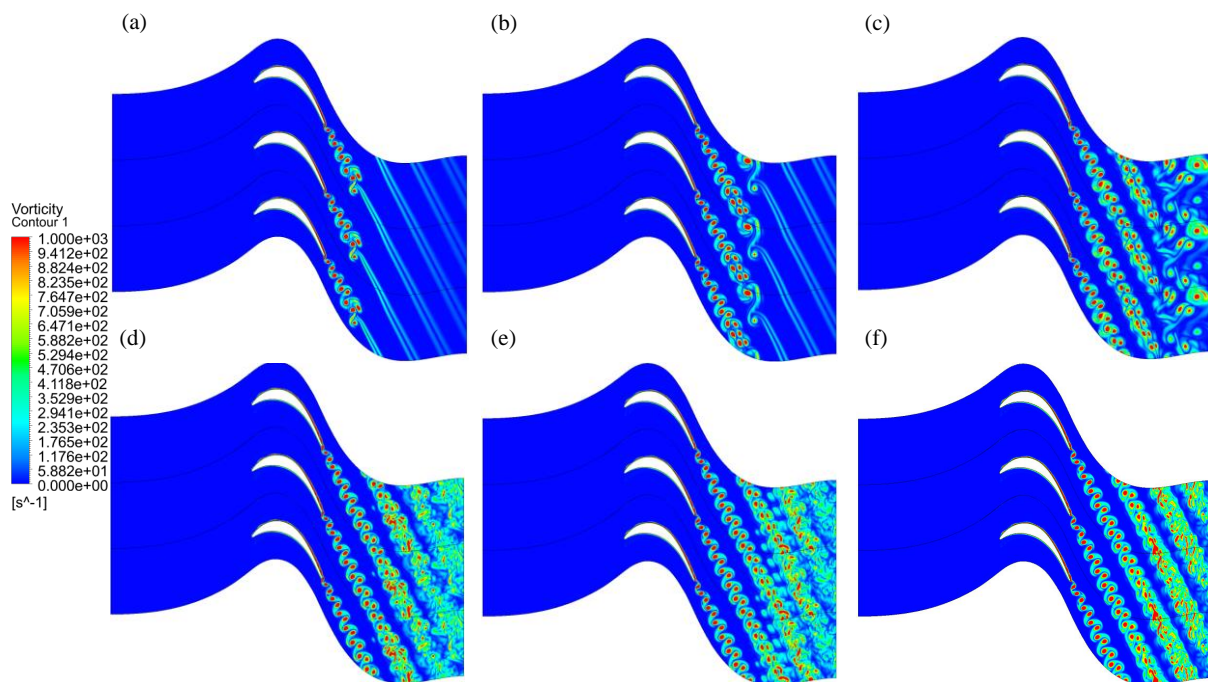

Figure 9. Instantaneous vorticity fields obtained after: (a) 5 vibration periods, (b) 10 vibration periods, (c) 20 vibration periods, (d) 30 vibration periods, (e) 40 vibration periods, and (f) 50 vibration periods
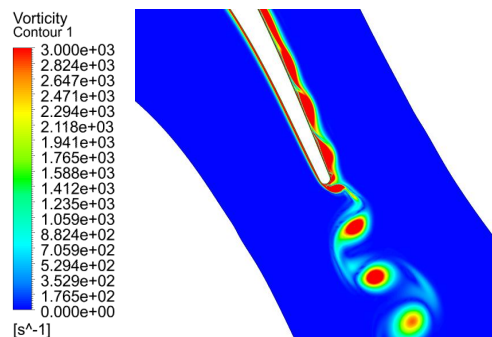

Figure 10. Close-up view of the vorticity around the trailing edge of the blade after 50 vibration periods

21

The close-up view of the vorticity around the trailing edge of the blade after 50 vibration periods is shown in Fig. 10 to highlight the flow structures near the trailing edge. The outer bound of the colourmap is increased to be able to clearly see the flow separation and vortex structures in this region. As seen, the rolling up of separated shear layer and flow recirculation, similar to KH rolls, are observed on the suction side near the trailing edge before shedding from the trailing edge. A little fluctuation in pressure distribution near the trailing edge, which was seen in Fig. 7, is associated with this phenomenon.

Figure 11 compares well-developed flow fields from the stationary blade case and the vibrating blade case after 50 vibration periods in which the differences between the two cases can be observed. As seen, the flow field is dominated by the blade motion in the latter case. Furthermore, the flow structures are highly unsteady, more organised and stronger in the vibrating blade case, compared to the stationary blade case, due to the periodic movement of the blade. Therefore, the conclusion can be drawn from these observations that the blade vibration has a significant impact on the flow, and the unsteady flow structures are strongly influenced and controlled by the blade vibration frequency and amplitude.
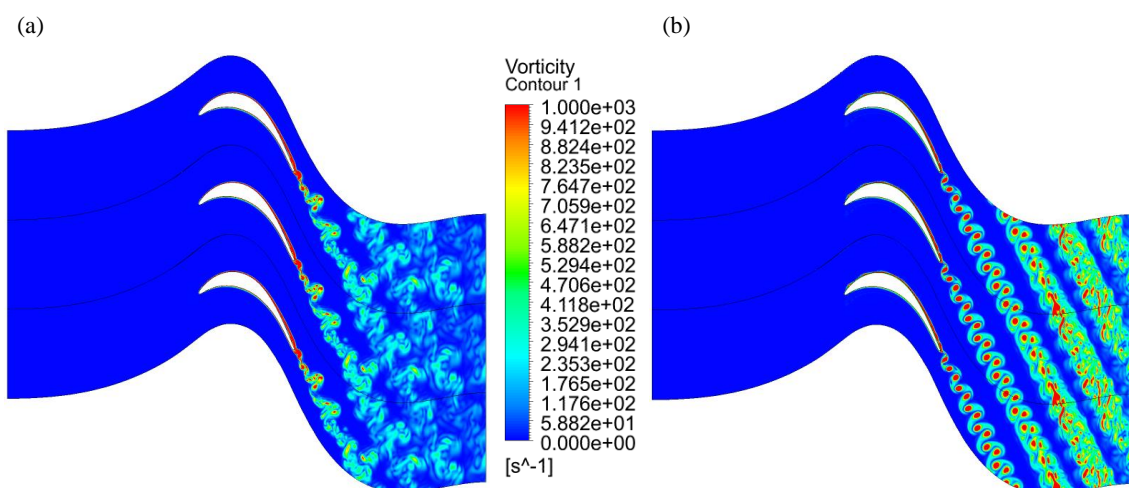

Figure 11. The comparison of vorticity fields between (a) the stationary blade case and (b) the vibrating blade case after 50 vibration periods

22

In addition to the time domain method, the harmonic balance method is also used in this study using different harmonics to determine the capability of the harmonic balance method on analysing the aeroelasticity and unsteady flow inside a modern LPT at a low Reynolds number involving the highly unsteady vorticity and wake. Figure 12 presents the vorticity developed from the trailing edge of the blade within the initial vibration periods obtained from the time domain method and the harmonic balance method using different harmonics. As shown, the vorticity predicted by using 1 harmonic and 3 harmonics are not comparable to that of the time domain method which indicates that 3 harmonics are not even enough to resolve the flow structures. It is seen that using 5 harmonics produces similar vortex structures as the time domain method. However, none of them seems to have accurately captured the flow leaving from the trailing edge. Although the flow resolution will be better with higher orders of harmonics, this will also increase the requirement of computational resources by a significant factor which could also be beyond the capabilities of supercomputers. Nevertheless, it can be said that at least 5 harmonics are required to resolve the necessary flow structures due to the interaction between the unsteady flow and the blade structure vibration inside an LPT.
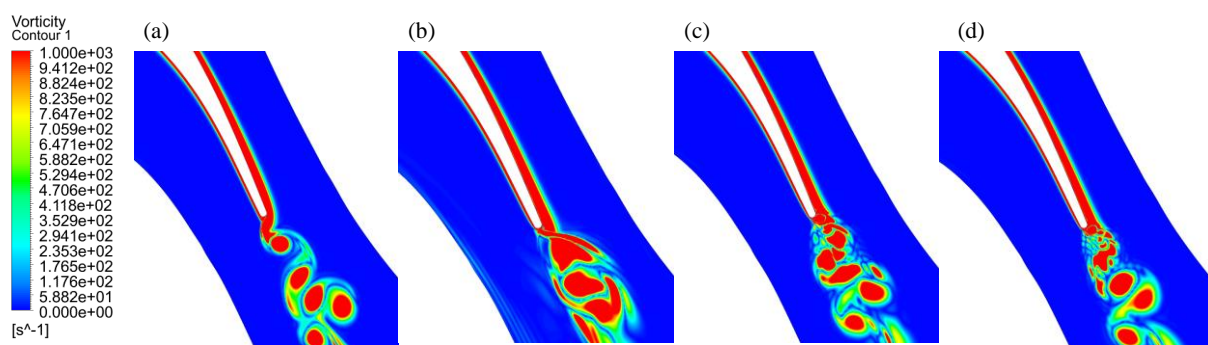

Figure 12. The comparison of vorticity fields captured by (a) the time domain method and the harmonic balance method using (b) 1 harmonic, (b) 3 harmonics, (c) 5 harmonics

One of the important parameters in the aeromechanical analysis of turbomachines is the aerodynamic damping value, which is used to determine whether the blade vibration is stable.

The URANS models are traditionally employed by the existing high-fidelity aeroelasticity solvers and they are still widely used in the industry to compute aerodynamic damping as they are computationally less expensive. In this paper, the URANS simulation is also carried out in addition to the DNS simulation to examine the capability of the URANS model on not only computing the aerodynamic damping but also predicting the behaviour of the unsteady flow after interaction with the blade structure. The k-omega SST turbulence model is used for the URANS computation. For a direct comparison to the DNS computation, the same time-step and total run time are used. The aerodynamic damping values computed from both methods are presented in Table 1. It is seen that the aerodynamic damping predicted by the URANS model is comparable to that of the DNS model. However, as shown in Fig. 13 and 14, the URANS model is, in fact, unable to not only capture the flow separation but also resolve the unsteady flow accurately compared to the DNS model. Therefore, it is evident that the use of URANS model is theoretically problematic when the highly unsteady flow and the flow separation are the main concerns, and it is unable to provide the physical understanding behind the complex fluid-structure interaction process which is essential to study the wake interaction between the blade rows and the transient flow. Figure 15 describes the total wall work distribution on the blade which shows that the blade has a dominant stabilizing effect on the suction surface.

Table 1. The comparison of aerodynamic damping values obtained using the DNS and URANS models

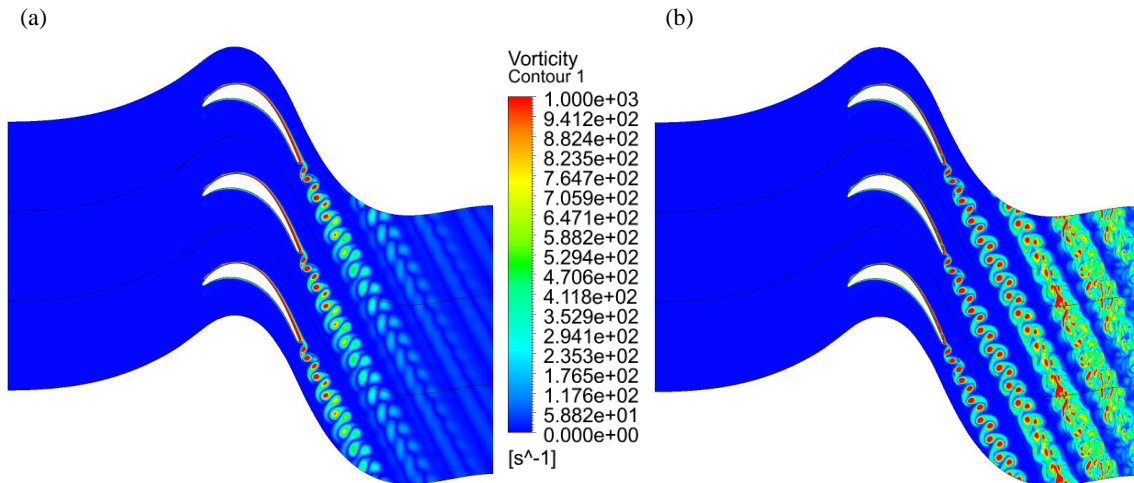| Type of Model	Aerodynamic Damping
DNS	0.056
URANS	0.055

Figure 13. The comparison of vorticity fields between (a) the URANS model and (b) the DNS model
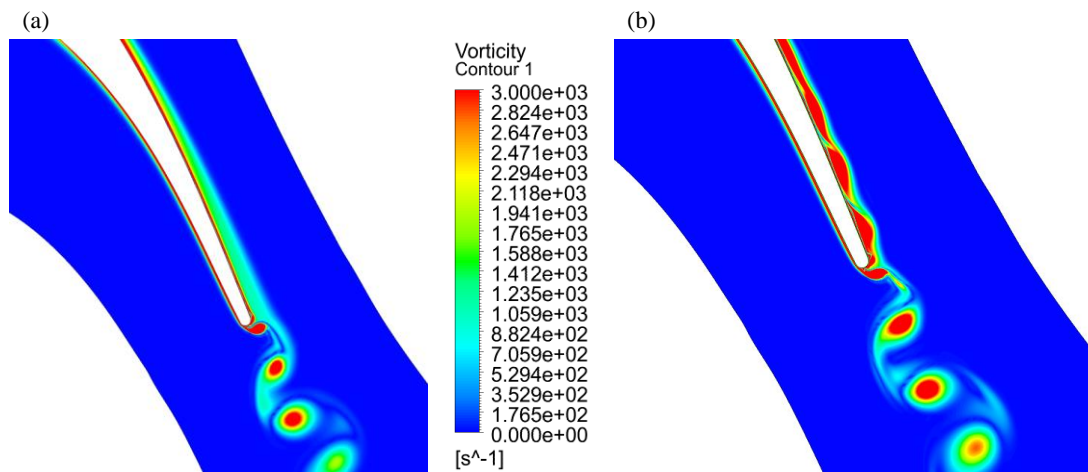

Figure 14. The comparison of close-up views of the vorticity around the trailing edge between (a) the URANS model and (b) the DNS model
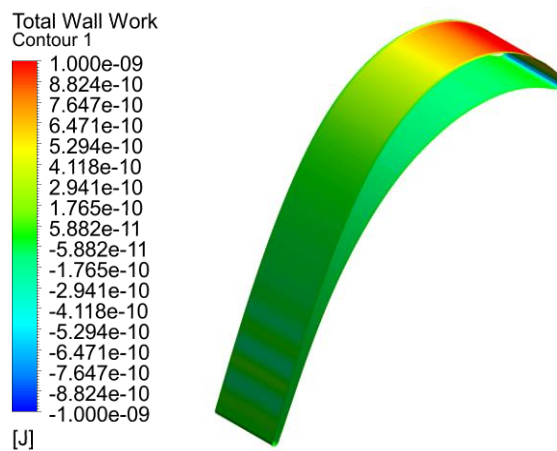

Figure 15. Total wall work distribution on the surfaces of T106A turbine blade *(positive values represent stabilizing effect and negative values represent destabilizing effect)*

4.3 Computational Cost

The simulations discussed in this paper are all performed on an HPC cluster. Each node consists of Dual Intel Xeon E5-2680 v4 14 core 2.4GHz CPU, 64GB RAM, 120GB SSD. Total of 56 processors are used for the time domain method whereas 24 processors can only be used with the harmonic balance method due to extremely large memory requirement. This can be noted as the limitation of the harmonic balance method. The computational costs with respect to the total processors used for each case are listed in Table 2. The harmonic balance method solves significantly faster than the time domain method. The solution takes longer with higher orders of harmonics. It takes approximately 26 hours on 24 processors with the harmonic balance method using 5 harmonics whereas it takes about 10 days on 56 processors using the time domain method.

Table 2. The total computational cost of each numerical method with respect to total processors used

Method	No. of Processors	Computation time
Time Domain Method	56	238 hours
Harmonic Balance Method using 1 Harmonic	24	5 hours
Harmonic Balance Method using 3 Harmonics	24	15 hours
Harmonic Balance Method using 5 Harmonics	24	26 hours

5. CONCLUSIONS

In this paper, the numerical investigation of the interaction between the transient flow and the blade structure vibration in a modern LPT is presented. A high-fidelity DNS method is used for flow simulations. First of all, the CFD model used in this paper is validated against the experiment as well as the previous DNS simulations in terms of time-averaged pressure coefficient distribution, wake profile and wall shear stress. Using the validated CFD model, the forced response and flutter instability in this turbine is investigated. Results obtained show that a slight difference in time-averaged pressure distribution is seen between the vibrating blade

case and the stationary blade case whereas a significant difference is noticed between the two cases in terms of wake profiles. Negative and positive wake profiles with higher magnitudes are observed in the vibrating blade case. Visualisation of the flow structures indicates that the flow is highly distorted by the blade structure motion and the evolution of vortex structures are directly associated with the blade vibration. The breaking down and mixing up of vortex structures are identified after about 30 vibration periods leading to the highly unsteady and completely turbulent flow in the downstream region. The flow structures and vorticity fields are more organized and stronger in the vibrating blade case. KH rolls like vortex structures are also seen on the suction surface near the trailing edge. Therefore, a conclusion can be drawn from these observations that the unsteady flow inside an LPT is highly influenced by the blade structure vibration, and the shape and the size of the vortex structures are determined by the frequency and amplitude of the blade vibration.

The URANS computation is also conducted in this paper and the results are compared to that of the DNS computation. It is found that the aerodynamic damping value predicted from the URANS model is comparable to that of the DNS model. However, the URANS model is unable to capture the flow separation and the unsteady flow accurately resulting in lack of flow information to understand the physics behind the fluid-structure interaction process which is very important for LPTs and essential to study the wake interaction between the blade rows. Thus, it can be concluded that the URANS models are not preferable for the study of LPTs involving highly unsteady flow.

In addition to the time domain method, the harmonic balance method using different harmonics is also used in this paper to determine the capability of the method in analysing aeroelasticity and the transient flow inside a modern LPT. Results show that at least 5 harmonics are required

to resolve the necessary flow structures. In terms of computation time, the time domain method requires a considerably larger amount of CPU time compared to the harmonic balance method. However, the harmonic balance method requires a great number of computational resources and the use of higher orders of harmonics is quite limited.

REFERENCES

1. Kadhim H.T, Rona A, Paul Gostelow J, Leschke K (2018) Optimization of the non-axisymmetric stator casing of a 1.5 stage axial turbine; International Journal of Mechanical Sciences; 136: 503–514.

2. Jung S.Y, Kim J.J, Park H.W, Lee S.J (2018) Comparison of flow structures behind rigid and flexible finite cylinders; International Journal of Mechanical Sciences; 142–143: 480–490.

3. Hodson H, Howell R (2005) The role of transition in high-lift low-pressure turbines for aeroengines; Progress in Aerospace Sciences; 41(6): 419–454.

4. Himmel C.G (2010) Ultra-High lift blades for Low Pressure Turbines; PhD Thesis, University of Cambridge.

5. Shi W, Yi W, Ji L (2018) Effect of inlet total pressure non-uniform distribution on aerodynamic performance and flow field of turbine; International Journal of Mechanical Sciences; 148: 714–729.

6. Hodson H, Howell R (2005) Blade Row Interactions, Transition, and High-Lift Aerofoils in Low-Pressure Turbines; Annu. Rev. Fluid Mech.; 37: 71–98.

7. Cull J, Hodson H (2011) Unsteady boundary-layer transition in low-pressure turbines; J. Fluid Mech.; 681(1): 370–410.

8. Panovsky J, Kielb, R.E (2000) A Design Method to Prevent Low Pressure Turbine Blade Flutter; J. Eng. Gas Turbines Power; 122(1): 89-98.

9. Waite J.J, Kielb R.E (2014) Physical Understanding and Sensitivities of Low Pressure Turbine Flutter; J. Eng. Gas Turbines Power; 137(1): 012502.

10. Waite J.J, Kielb R.E (2015) The Impact of Blade Loading and Unsteady Pressure Bifurcations on Low-Pressure Turbine Flutter Boundaries; ASME. J. Turbomach.; 138(4): 041002.

11. Corral R, Vega A (2016) The Low Reduced Frequency Limit of Vibrating Airfoils—Part I: Theoretical Analysis; ASME J. Turbomach.; 138(2): 021004.

12. Dowell E (2015) A Modern Course in Aeroelasticity; Springer; ISBN 978-3-319-09452-6.

13. Ning W, He L (1998) Computation of Unsteady Flows Around Oscillating Blades Using Linear and Nonlinear Harmonic Euler Methods; ASME J. Turbomach; 120(3): 508-514.

14. Hall K, Lorence C (1993) Calculation of Three-Dimensional Unsteady Flows in Turbomachinery Using the Linearized Harmonic Euler Equations; ASME J. Turbomach.; 115(4): 800-809.

15. Hall K, Thomas J, Clark W (2002) Computation of Unsteady Nonlinear Flows in Cascades Using a Harmonic Balance Technique; AIAA Journal; 40(5): 879-886.

16. He L (2008) Harmonic Solution of Unsteady Flow Around Blades with Separation; AIAA Journal; 46(6): 1299-1307.

17. Rahmati M.T, He L, Wells R.G (2010) Interface treatment for harmonic solution in multi-row aeromechanic analysis; ASME Turbo Expo 2010: Power for Land, Sea, and Air (pp. 1253-1261); American Society of Mechanical Engineers.

18. Rahmati M.T, He L, and Li Y.S (2012) Multi-row interference effects on blade aeromechanics in compressor and turbine stages; 13th International Symposium on Unsteady Aerodynamics, Aeroacoustics and Aeroelasticity of Turbomachines (ISUAAAT); September 11-14, Tokyo, Japan.

19. Rahmati M.T, He L, and Li Y.S (2016) The Blade Profile Orientations Effects on the Aeromechanics of Multirow Turbomachines; J. Eng. Gas Turbines Power;137 (6): 062606.

20. Rahmati M.T, He L, Wang D.X, Li Y.S, Wells R.G, Krishnababu S.K (2014) Nonlinear Time and Frequency Domain Methods for Multirow Aeromechanical Analysis; ASME J. Turbomach.; 136(4): 041010.

21. Win Naung S, Rahmati M.T, Farokhi H (2019) Aerodynamic Analysis of a Wind Turbine with Elevated Inflow Turbulence and Wake using Harmonic Method; Proceedings of the ASME 2019 38th International Conference on Ocean, Offshore and Arctic Engineering (OMAE2019); June 9-14, Glasgow, Scotland.

22. Win Naung S, Rahmati M.T, Farokhi H (2019) Aeromechanical Analysis of Wind Turbines using Non-linear Harmonic Method; Proceedings of the ASME 2019 38th International Conference on Ocean, Offshore and Arctic Engineering (OMAE2019); June 9-14, Glasgow, Scotland.

23. Brearda C, Greenb J.S, Vahdatia M, Imreguna M (2001) A non-linear integrated aeroelasticity method for the prediction of turbine forced response with friction dampers; International Journal of Mechanical Sciences; 43: 2715–2736.

24. D'Alessandro V, Montelpare S, Ricci R, Zoppi A (2018) Fluid–dynamic analysis of a multi–blade gravity damper; International Journal of Mechanical Sciences; 135: 14–22.

25. Zamiri A, Chung J.T (2017) Ability of URANS approach in prediction of unsteady turbulent flows in an unbaffled stirred tank; International Journal of Mechanical Sciences; 133: 178–187.

26. Tucker P.G (2001) Computation of unsteady internal flows; Norwell MA: Kluwer Academic Publishers.

27. Tucker P.G (2005) Computation of unsteady turbomachinery flows: Part 1—Progress and challenges; Progress in Aerospace Sciences; 47(7): 522-545.

28. Tucker P.G (2013) Unsteady computational fluid dynamics in aeronautics; Springer; ISBN 978-94-007-7048-5.

29. Ghasemi E, Bararnia H, Soleimanikutanaei S, Lin C.X (2018) Direct numerical simulation and analytical modeling of electrically induced multiphase flow; International Journal of Mechanical Sciences; 142–143: 397–406.

30. Liu Y, Ma D, Fu B, Li Q, Zhang C (2019) Direct numerical simulation of fine flow structures of subsonic-supersonic mixing layer; Aerospace Science and Technology; 95: 105431.

31. Oginoa K, Mamori H, Fukushimac N, Fukudomea K, Yamamotoa M (2019) Direct numerical simulation of Taylor–Couette turbulent flow controlled by a traveling wave-like blowing and suction; International Journal of Heat and Fluid Flow; 80: 108463.

32. Watanabe T, Zhang X, Nagata K (2019) Direct numerical simulation of incompressible turbulent boundary layers and planar jets at high Reynolds numbers initialized with implicit large eddy simulation; Computers and Fluids; 194: 104314.

33. Zhu H, Liu W, Zhou T (2020) Direct numerical simulation of the wake adjustment and hydrodynamic characteristics of a circular cylinder symmetrically attached with fin-shaped strips; Ocean Engineering; 195: 106756.

34. Stadtmüller P (2001) Investigation of wake-induced transition on the LP turbine cascade T106A-EIZ; DFG-Verbundproject Fo 136/11, Version 1.0.

35. Wang Y.F, Chen F, Liu H.P, Chen H.L (2014) Large eddy simulation of unsteady transitional flow on the low-pressure turbine blade; China Technol. Sci.; 57(9): 1761–1768.

36. Garai A, Diosady L.T, Murman S.M, Madavan N.K (2016) DNS of Low-Pressure Turbine Cascade Flows With Elevated Inflow Turbulence Using a Discontinuous-Galerkin Spectral-Element Method; Proceedings of the ASME Turbo Expo 2016: Turbomachinery Technical Conference and Exposition; June 13–17, Seoul, South Korea.

37. Wissink J.G (2003) DNS of separating, low Reynolds number flow in a turbine cascade with incoming wakes; Int. J. of Heat and Fluid Flow; 24(4): 626-635.

38. Wissink J.G, Rodi, W (2006) Direct Numerical Simulations of Transitional Flow in Turbomachinery; ASME J. Turbomach.; 128 (4): 668–678.

39. Michelassi V, Wissink J, Rodi W (2002) Analysis of DNS and LES of Flow in a Low Pressure Turbine Cascade with Incoming Wakes and Comparison with Experiments; Flow, Turbulence and Combustion; 69: 295–330.

40. Ranjan R, Deshpande S.M, Narasimha R (2016) A high-resolution DNS study of compressible ow past an LPT blade in a cascade; arXiv:1611.09746.

41. Ranjan R, Deshpande S.M, Narasimha R (2017) New insights from high-resolution compressible DNS studies on an LPT blade boundary layer; Computers and Fluids; 153: 49–60.

42. Sandberg R.D, Michelassi V, Pichler R, Chen L, Johnstone R (2015) Compressible Direct Numerical Simulation of Low-Pressure Turbines—Part I: Methodology; ASME. J. Turbomach.; 137(5): 051011.

43. Michelassi V, Chen L, Pichler R, Sandberg R.D (2015) Compressible Direct Numerical Simulation of Low-Pressure Turbines—Part II: Effect of Inflow Disturbances; ASME. J. Turbomach.; 137(7): 071005.

44. Kajishima T, Taira K (2017) Computational Fluid Dynamics: Incompressible Turbulent Flows; Springer; ISBN 978-3-319-45304-0.

45. Huang X.Q, He L, Bell D.L (2009) Experimental and Computational Study of Oscillating Turbine Cascade and Influence of Part-Span Shrouds; Journal of Fluids Engineering; 131: 051102-1.

46. Buchwald P, Farahmand A, Vogt D.M (2018) On the Influence of Blade Aspect Ratio on Aerodynamic Damping; Proceedings of the 15th International Symposium on Unsteady Aerodynamics, Aeroacoustics & Aeroelasticity of Turbomachines; September 24-27, University of Oxford, UK.